# USE OF POTENTIAL FLOW STATE-SPACE INFLOW MODELING FOR MASS SOURCE ROTORS

**Ke Yu** and **David A. Peters**
Department of Mechanical Engineering
Washington University, Campus Box 1185, St. Louis, MO 63130-4899, USA

## Abstract

In the field of rotorcraft dynamics, it is significant to all that the induced inflow field is well understood and modeled. A large number of methodologies have been developed in the past years, among which the state-space model is highly recognized for its outstanding advantage in real-time simulation, preliminary design, dynamic eigenvalue analysis and etc. Recent studies have shown success in representing the induced flow field everywhere above the rotor plane even with mass source terms as long as they have zero net flux. Nevertheless, non-zero net mass influx is expected in numerous situations, such as ground effect, mass source rotors, etc; and the incapability of previous models keeps the methodology's utilization in these cases. This work presents an extended potential flow state-space model derived from potential flow momentum equation by means of Galerkin approach. The induced velocity and pressure perturbation are expanded in terms of closed-form, time-dependent coefficients and space-dependent associated Legendre functions and harmonics. Non-zero net mass flux terms are represented by the involvement of associated Legendre functions with equal degrees and orders. Validation, as well as discrepancies, of the inclusion of such terms is investigated. Numerical simulation of frequency responses in axial and skew-angle flight are presented and compared with exact solutions obtained by convolution integral. Also the study shows that, unlike other pressure distribution responses, non-zero mass influx exhibits high sensitivity to the choice of number of states in the velocity expansion. Error analyses are performed to show this sensitivity.

## Introduction

An understanding of the flow field during flight is necessary in order to make design improvements to the performance and maneuverability of a helicopter. This is a crucial topic in preliminary design and flight test. As with all other topics in research, there is more than one approach to the understanding of the flow field. CFD is probably the most fundamental method available. Nevertheless, the flexibility of CFD is offset by the large computational effort and the difficulty in capturing free vorticity. Vortex lattice results are another approach with great utility, but they can often be computationally prohibitive for analyses that require real-time simulation or eigenvalues. In these cases, a finite-state model of the inflow is required. This paper concentrates on finite-state modeling.

Sissingh [1] first proposed a simple, first-harmonic inflow and lift distribution without any dependence on the radial position of the rotor blade. That model assumed an instantaneous relationship between perturbations of induced velocity and perturbations in thrust. Sissingh showed good correlation of predicted data with flight measurements. In the early 1970s, Ormiston and Peters [2] introduced the idea of expressing the induced flow in state-variable form. The first theory was a quasi-steady formulation with the assumption of a linear relationship between perturbations of inflow components and rotor thrust. This formulation represents the induced rotor inflow by a truncated Fourier series and assembles a theory that relates the inflow field at blades to the lift and circulation developed on the blades. This significantly simplifies the analysis of dynamic inflow. Peters later extended this model to the unsteady condition [3] by addition of the apparent mass of the inflow distributions. Though good correlations were obtained at axial or edgewise flow, a transition between these conditions was not allowed by this model.

In the 1980s, Peters and Pitt developed a linear, unsteady theory that relates transient rotor loads to the overall transient response of the rotor induced flow field [4-6]. This model is based on unsteady potential flow theory with the assumption that the total pressure due to a velocity field can be formed by superimposing the unsteady pressure and the static pressure of that field. Even though this theory proved to be practical and easy to use with good correlations, it is a low-order approximation and is limited to only the crudest wake description of uniform flow with one simple gradient. In 1987, Peters and He [7] turned to a higher-harmonic theory of dynamic inflow. The pressure distribution, as well as the inflow field, is extended to include an arbitrary number of harmonics and an arbitrary number of radial functions per harmonic. This new model gives excellent correlation on the rotor disc plane and in a more detailed fashion than the Pitt model. However, it obtains only the normal component of flow at the rotor disk and does not provide all three components of flow on and above the rotor disk plane. In addition, it cannot be applied to cases with mass injection at the rotor. In 2001, based on a two-dimensional model studied

by Nelson [8], Morillo extended the Peters-He Model to include an additional set of functions, which enabled the new model to remove most of the limitations of the previous model [9].

However, no net mass flow terms were considered in these models. Therefore, for helicopters with mass source rotors, as well as those undergoing ground effect could not be studied. This research reviews and extends Morillo's work, rather than builds new models, since a good correlation has already been established. Net mass flow components are considered in the flow field by presence of certain pressure terms. Numerical results are compared with those from convolution integration, and in some special cases, an exact solution in closed-form. Also, the influence of the choice of number of states, including number of discontinuous functions and mass injection functions, is investigated through error analysis. Optimized results of individual pressure distribution of net mass influx are obtained and compared to results from original formation.

## Notation

| | |
|---|---|
| $\hat{a}_n^m$ , $a_n^m$ | Velocity expansion coefficient |
| $\hat{b}_n^m$ , $b_n^m$ | Velocity expansion coefficient |
| $[\mathbf{D}]$ | Damping matrix |
| $E$ | Error norm |
| $H_n^m$ | Coefficient |
| $i$ | Imaginary number |
| $K_n^m$ | Legendre constant |
| $[\tilde{\mathbf{L}}]$ | Influence coefficient matrix |
| $[\mathbf{M}]$ | Mass matrix |
| $m$ | Order of Legendre function (Harmonic number) |
| $n$ | Degree of Legendre function (Polynomial number) |
| $P$ | Pressure |
| $P_n^m$ , $Q_n^m$ | Associated Legendre functions |
| $\bar{P}_n^m$ , $\bar{Q}_n^m$ | Normalized associated Legendre functions |
| $v$ | Velocity |
| $\chi$ | Inflow angle |
| $\delta_{ij}$ | Kronecker delta |
| $\Phi_n^m$ | Pressure potential function |
| $\nu$ , $\eta$ , $\bar{\psi}$ | Ellipsoidal coordinates |
| $\rho_n^m$ | Normalization factor |
| $\varsigma_n^m$ , $\sigma_n^m$ | Change of variable constant |
| $\tau_n^{mc}$ , $\tau_n^{ms}$ | Pressure expansion coefficient |
| $\xi$ | Inflow coordinate unit |
| $\Psi_n^m$ | Velocity potential function |

**Superscripts and Subscripts**

| | |
|---|---|
| $(\ )^c$ | Cosine terms |
| $(\ )^s$ | Sine terms |
| $(\ )^m$ | Harmonic number |
| $(\ )_n$ | Polynomial number |
| $(\ )_z$ | Axial component |

## Extended State-Space Model

A state-space model is developed with velocity perturbation and pressure perturbation expanded in series such that

$$P = -\sum_{m=0}^{\infty}\sum_{n=m}^{\infty}\left(\tau_n^{mc}\Phi_n^{mc} + \tau_n^{ms}\Phi_n^{ms}\right) \tag{1}$$

$$\bar{v} = \sum_{m=0}^{\infty}\sum_{n=m}^{\infty}\left(\hat{a}_n^m\bar{\nabla}\Psi_n^{mc} + \hat{b}_n^m\bar{\nabla}\Psi_n^{ms}\right) \tag{2}$$

where

$$\begin{cases}\Phi_n^{mc} = \Phi_n^m\cos\left(m\bar{\psi}\right) = \bar{P}_n^m\left(\nu\right)\bar{Q}_n^m\left(i\eta\right)\cos\left(m\bar{\psi}\right)\\ \Phi_n^{ms} = \Phi_n^m\sin\left(m\bar{\psi}\right) = \bar{P}_n^m\left(\nu\right)\bar{Q}_n^m\left(i\eta\right)\sin\left(m\bar{\psi}\right)\end{cases} \tag{3}$$

$$\begin{cases}\Psi_n^{mc} = \int_{\xi}^{\infty}\Phi_n^{mc}d\xi\\ \Psi_n^{ms} = \int_{\xi}^{\infty}\Phi_n^{ms}d\xi\end{cases} \tag{4}$$

$\bar{P}_n^m\left(\nu\right)$ and $\bar{Q}_n^m\left(i\eta\right)$ are normalized associated Legendre function of the first and second kind, respectively,

$$\bar{P}_n^m = \left(-1\right)^m\frac{P_n^m\left(\nu\right)}{\rho_n^m} \tag{5}$$

$$\bar{Q}_n^m = \frac{Q_n^m\left(i\eta\right)}{Q_n^m\left(i0\right)} \tag{6}$$

with

$$\left(\rho_n^m\right)^2 = \int_0^1\left[P_n^m\left(\nu\right)\right]^2 d\nu = \frac{1}{2n+1}\frac{\left(n+m\right)!}{\left(n-m\right)!} \tag{7}$$

$$Q_n^m\left(i0\right) = \begin{cases}\dfrac{\pi}{2}\left(-1\right)^{m+n+1}\left(i\right)^{n+1}\dfrac{\left(n+m-1\right)!!}{\left(n-m\right)!!} & n+m = even\\ \left(-1\right)^{m+n+1}\left(i\right)^{n+1}\dfrac{\left(n+m-1\right)!!}{\left(n-m\right)!!} & n+m = odd\end{cases} \tag{8}$$

$\tau_n^{mc}$ and $\tau_n^{ms}$, $\hat{a}_n^m$ and $\hat{b}_n^m$ are time-dependent pressure coefficients and velocity coefficients, respectively. These coefficients are governed by the final non-dimensionalized matrix-form momentum equation

$$\left[\mathbf{M}^c\right]\left\{\dot{a}_n^m\right\}+\left[\mathbf{D}^c\right]\left[\tilde{\mathbf{L}}^c\right]^{-1}\left[\mathbf{M}^c\right]\left\{a_n^m\right\}=\left[\mathbf{D}^c\right]\left\{\tau_n^{mc}\right\} \qquad (9)$$
$$m=0,1,2,3,\cdots, \quad n=m+1,m+2,m+3,\cdots.$$

with a change of variables from $\hat{a}_n^m$ to $a_n^m$

$$\left\{\Psi_n^{mc}\right\}^T\left\{\hat{a}_n^m\right\}=\left\{\sigma_n^m\Phi_{n+1}^{mc}+\varsigma_n^m\Phi_{n-1}^{mc}\right\}^T\left\{a_n^m\right\} \qquad (10)$$

where

$$\sigma_n^m=\frac{1}{K_n^m\sqrt{(2n+1)(2n+3)\left[(n+1)^2-m^2\right]}} \qquad (11)$$

$$\varsigma_n^m=\frac{1}{K_n^m\sqrt{(4n^2-1)(n^2-m^2)}} \qquad n\neq m \qquad (12)$$

and

$$K_n^m=\left(\frac{\pi}{2}\right)^{(-1)^{n+m}}H_n^m \qquad (13)$$

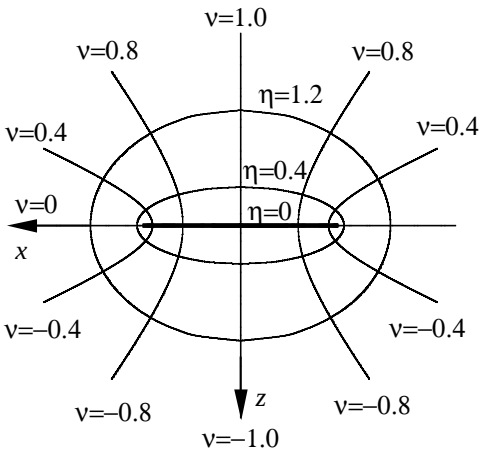


**Figure 1. Ellipsoidal coordinates viewed in x-z plane**

$$H_n^m=\frac{(n+m-1)!!(n-m-1)!!}{(n+m)!!(n-m)!!} \qquad (14)$$

Superscripts "*c*" in matrix notation imply these are cosine components of the complete equation. However, Eqs. (1) and (2) imply that the sine and cosine terms are completely decoupled, an identical set of equations of sine components could be written. The spatial variables are locations of investigation in an ellipsoidal coordinates system as shown in Fig. 1. $\bar{\psi}$ is the azimuthal angle measured counterclockwise from negative *x*-axis in *x*-*y* plane.

The state-space model represented by Eq. (9) yields excellent correlation in all three components of velocity perturbations everywhere in the flow field above the rotor plane for various pressure distributions, which are determined uniquely by rotor conditions (i.e., number of blades, sectional lift, blades' rotating frequency and etc). However, the net mass flow terms, which are presented by associated Legendre functions with equal orders and degrees, i.e., *m*=*n*, in pressure expansions, are not adopted in formulation. This is based on the fact that these terms yield infinite kinetic energy in the flow field. Without losing generality, assume a pressure distribution $P=-\Phi_0^0$. The vertical component of induced velocity yields

$$v_z=\Phi_0^0=\bar{P}_0^0(\nu)\bar{Q}_0^0(i\eta) \qquad (15)$$

and therefore

$$v_z=\begin{cases}\bar{P}_0^0(\nu)=1 & \text{on-disc}\\ \bar{Q}_0^0(i\eta)=\dfrac{2}{\pi}\tan^{-1}\left(\dfrac{1}{\eta}\right) & \text{off-disc}\end{cases} \qquad (16)$$

For off-disc area, if Taylor series is used for large $\eta$

$$v_z=\frac{2}{\pi}\tan^{-1}\left(\frac{1}{\eta}\right)=\frac{2}{\pi}\left(\frac{1}{\eta}-\frac{1}{3\eta^3}+\cdots\right) \qquad (17)$$

then the kinetic energy per unit mass of the induced flow crossing the off-disc rotor plane ($\nu=0$, $a\le\eta<\infty$) is that

$$T=\frac{1}{2}\iint_s v_z^2\,ds=\frac{4}{\pi}\int_a^\infty\left(\frac{1}{\eta}-\frac{1}{3\eta^3}\right)^2\eta\,d\eta=\infty \qquad (18)$$

Equation (18) fully expresses the major discrepancy of including non-zero net mass flux terms in the model: Involvement of net mass flux terms, which happens in tremendous practical cases, will theoretically introduce infinite energy in the flow field. However, the infinite result is true

based on two assumptions: the media field does not dissipate energy at all, and the whole system, including the media field to a distance of infinity, is in steady state. In reality, first of all, damping of air, even though very small under the condition of helicopter operating, will actually dissipate the energy and the induced velocity decreases much faster away from the rotor than those shown in Eq. (17). And secondly, the operating period of helicopter is not infinite. Furthermore, the study of induced flow is not the final goal in the study of helicopter's performance – the ultimate goal is to see how it affects the behavior of helicopter blades, fuselage or personnel on the ground if it is close to the ground. Therefore, the most important concern is the area on or close to the actuator disc. Based on this aspect, if the results have good correlation at on-disc, or close-to-disc, area, the involvement of net mass flux could be tolerated.

On the other hand, to avoid inconvenience of numerical integration of velocity potentials, the variable change shown in Eq. (10) prohibits any $m=n$ terms in velocity expansion in Eq. (2). However, this prohibition is only for the mass matrix $\left[\mathbf{M}^c\right]$ and the influence coefficient matrix $\left[\tilde{\mathbf{L}}^c\right]$ and has no effect on the damping matrix $\left[\mathbf{D}^c\right]$, which is the coefficient matrix of the pressure coefficient vector on the right hand side of Eq. (9). Therefore, it might be possible to include $m=n$ in $\tau_n^m$ but not in the velocity potentials.

To include net mass flux terms, i.e., $\bar{P}_m^m(\nu)$ and $\bar{Q}_m^m(i\eta)$, in the pressure distribution, the damping coefficient matrix $\left[\mathbf{D}^c\right]$ on the right hand side of Eq. (9) will be required to have extra columns. Based on the goal that the new model should reduce to Eq. (9) if net mass flux terms are not considered, these new entrees are desired to follow the same formulation of $\left[\mathbf{D}^c\right]$. The formulation of damping matrix $\left[\mathbf{D}^c\right]$ follows that

$$D_{jn}^{rm} = \frac{1}{K_n^m}\delta_{jn}$$
$$r=m,\quad j+r=\text{odd},\quad n+m=\text{odd} \qquad (19)$$
$$r=m,\quad j+r=\text{even},\quad n+m=\text{even}$$

$$D_{jn}^{rm} = \frac{2}{\pi\sqrt{H_n^m H_j^m}}\frac{\sqrt{(2j+1)(2n+1)}}{(j+n+1)(j-n)}(-1)^{(j+3n-1)/2}$$
$$r=m,\quad j+r=\text{even},\quad n+m=\text{odd} \qquad (20)$$
$$r=m,\quad j+r=\text{odd},\quad n+m=\text{even}$$

$$D_{jn}^{rm}=0 \qquad r\neq m \qquad (21)$$

where $r$ and $j$ are indices introduced by trial functions.

Indeed, the formulation of damping matrix does not exclude any equal degree-order associated Legendre functions either in its closed-form representation or derivation; and therefore, the net mass flux terms could be included in the pressure distribution. Considering that the matrices on the left hand side have to be square, the extended momentum equation is expressed as

$$\left[\mathbf{M}^c\right]\left\{\dot{a}_n^m\right\}+\left[\mathbf{D}^c\right]\left[\tilde{\mathbf{L}}^c\right]^{-1}\left[\mathbf{M}^c\right]\left\{a_n^m\right\}=\left[\bar{\mathbf{D}}^c\right]\left\{\tau_n^{mc}\right\} \qquad (22)$$

where $\left[\bar{\mathbf{D}}^c\right]$ is the extended damping matrix.

## Error analysis and simulation

The validity of the proposed state-space model, Eq. (22), is investigated by an error analysis. In this study, error is defined by

$$E^2=\frac{\int_A^B\left(|v_s-v_e|^2/\sqrt{1+\eta^2}\right)dr}{\int_A^B\left(|v_e|^2/\sqrt{1+\eta^2}\right)dr} \qquad (23)$$

where $v_s$ and $v_e$ are velocity perturbations from state-space model and convolution/closed-form solution, respectively. $r$ is the radial location, $A$ and $B$ are range of desired area of investigation. Since the accuracy of the model is of less importance off the disc, errors at location are multiplied by weigh coefficient $1/\sqrt{1+\eta^2}$, therefore, the further from the disc, the less error is counted in the analysis. And from this point, for the sake of convenience, $m+n$=even and $m+n$=odd terms will be called even and odd terms, respectively.

The previous Peters-He model suggests that the state-space model yields exact solution at edge-wise inflow if there are no even terms in the velocity expansion. Morillo expanded the model to include mass injection terms in pressure expansion, which demands involvement of even as well as odd terms in velocity. Based on the fact that the net-mass flow terms are special cases of even terms in the excitation, the involvement of even terms in the velocity expansion is also inherited. However, it is intuitive that the number of even terms will change the correlation with exact solution. Verification of this assumption is done by error analyses with various numbers of even terms in the state-space model. In this study, the number of even and odd terms is represented by the number of terms in the zeroth harmonic, that is, how many odd or even terms with $m$=0 are included.

For all of the illustrations shown, the pressure distribution is such that

$$P = -\Phi_m^m = -\bar{P}_m^m(\nu)\bar{Q}_m^m(i\eta)\cos(m\bar{\psi}) \qquad (24)$$

To exam the generality of proposed model, various excitation frequencies, as well as skewed angles along with different pressure distribution, are evaluated and discussed.

Figure 2 shows an example of error analysis for the pressure distribution $P = -\Phi_0^0$ with zero and infinite frequencies during axial flow. 2(a) shows the analysis with equal numbers of odd and even terms in the model, while 2(b) shows the effect of number of even terms in the model as the number of odd terms is fixed at 22. From 2(a) and 2(b), it is shown that the precision of results follows a rather smooth trend within a certain range of number of states that yields convergence. Within that range, the precision intends to increase with more terms included. Numerical simulation verified that beyond the range of convergence, (for example, number of states greater than 20 as shown in 2(a)), the convergence starts to break down and collapse rapidly if the number of states goes even higher. However, plots 2(c) and 2(d) are not following the same pattern. The accuracy of simulation keeps oscillating with little change in the number of states, undergoing more like a saw-tooth action. This behavior starts to appear with increase in either the frequency or the skewed-angle of flight. More simulation results verified that increase of frequency or skew angle shrinks the range of convergence. If the skew angle is changed, the number of even terms included becomes more and more important to the model's convergence. Some of these phenomena, like the increase of skew angle decreases the range of convergence, agree with that of zero net mass flow pressure distributions. But the saw-tooth behavior, or in another words, sensitivity with the number of states, is not seen before.

Figures 3 – 7 illustrate the on-disc optimized frequency responses of pressure distribution $P = -\Phi_0^0$ with various system configurations. In all plots, red circles are results from the convolution integral; blue triangles are results from closed-form solutions, which are available in limited cases; and black dots represent results of the proposed state-space model by Galerkin approach.

From Figs. 2(a) and 2(b) it is observed that when the odd terms and even terms are all 11 in the zeroth harmonic, this state-space model yields the highest accuracy of zero frequency response with respect to the exact solution. Numerical verification plotted in Fig. 2 shows, even though it is the optimal choice, visible errors still exist in both on-disc and off-disc area. As discussed, the velocity expansion excludes any terms with $m = n$, in which $m = n = 0$ is an extreme case. Notice if the pressure distribution is $P = -\Phi_0^0$, From Eq. (16), the closed-form solution of the z-component of on-disc velocity perturbation is uniform. However, there is no function in the velocity expansion that has property of uniformity on-disc. In a general sense, it requires a large number of terms in the velocity expansion to yield a good approximation. On the other hand, error analysis suggests that the convergence collapses after the number of states goes beyond a certain range. These two facts basically contribute to this error shown in Fig. 3(a). On the off-disc area, the Galerkin approach decays into the far field faster than the exact solution. This is expected and has been discussed in the previous section.

Figure 4 is the frequency response for infinite frequency. Based on the fact that the response actually becomes zero in such case, $\omega\nu_i$, $i = z, r, \bar{\psi}$, is plotted instead. It shows that the on-disc and far off-disc areas have good correlation with exact solution, yet relatively large oscillations appear at the edge of actuator. This is a consequence of using continuous expansion functions approximate a continuous velocity expansion.

Based on individual error analyses, optimized results of frequency response under various conditions are obtained and plotted in Figs. 5 – 7. Figure 5 shows the response one disc radius above the rotor plane in axial flow. Again it is noticed that the error is obvious and somewhat consistent, but it is of the same order as the off-disc error in Fig. 1(a).

Figure 6 shows the response at zero frequency in skewed flight. Considering that the vortices do not die out in the skewed wake, the induced flow will be larger in the trailing edge. Morillo showed that, in skewed flow, the number of even terms should be reduced.. However, it is also desired to have certain number of even terms in the velocity expansion because of the inclusion of even terms in the pressure distribution. A compromise could be found, but the error off-disc especially at the trailing edge is amplified. The accuracy of the model is evaluated on-disc in this research and indeed Fig. 6 shows that to a good extent. In further research, an overall error analysis could be performed to find another optimized number of states to give better correlation off-disc, with certain accuracy loss in the on-disc area.

Figure 7 shows response of a higher frequency, skewed-angle flight. Despite all the reasons discussed in Fig. 6, Fig. 7 shows good correlations in all four non-zero components. This is a direct result of increase of excitation frequency. For any non-zero frequency, the response is that

$$\{\bar{\mathbf{x}}\} = [\mathbf{B} + i\omega\mathbf{A}]^{-1}\{\bar{\boldsymbol{\tau}}\} \qquad (25)$$

and the error, if any, is decreased by factor of

$$\eta = \frac{|\mathbf{B}|}{|i\omega\mathbf{A} + \mathbf{B}|} \tag{26}$$

As long as the state-space model is within convergence range, the increase of frequency always plays a role reducing the error.

For purposes of illustration of generality of the model, Figs. 8 and 9 are presented to show the responses of pressure distribution $P = -\Phi_1^1$ with zero and infinite frequencies.

From all the plots, it can be seen that the radial components always have good correlation with exact solution, even when the axial components yields large error. In cases of on-disc optimization, the low power radial function will decrease off-disc errors and therefore yields better correlations.

## Conclusion

It is shown that the proposed state-space model is capable of treating non-zero net mass flux terms in the pressure distribution. The discrepancy is discussed and validation is performed through error analyses and numerical verifications. Based on the results obtained, the following conclusions are made

1) The proposed state-space with extended damping matrix is capable of including non-zero mass flux terms in the pressure distribution. The fact that these terms yield infinite kinetic energy is considered. Based on realistic situation, this discrepancy is discarded and numerical results agree with that in reality.
2) The model has the disadvantage that the net mass flux terms give sensitivity to the model. Even though individual net mass influx could be treated precisely, the combination of more than one flux term could result in unreliable result. Further work needs to be done in this subject.
3) The convergence of model is not ideal with low frequency, large skew-angle flight. Error on the trailing edge becomes significant in these cases. A correction factor is needed in skewed angle condition.
4) A trade-off sometimes exists during optimization. The choice of number of states is based on the importance of location of induced flow. On-disc optimization usually gives excellent correlation on-disc, but could lose convergence off-disc. If an overall area optimization is adopted, the excellence of on-disc correlation will be reduced.

Other adjustments and calibrations are always of interest to improve the proposed model. However, a major future work is to apply the complete state-space model with blade element theory and blade dynamics, and experimented results if available, to verify the complete validity of model.

## Reference


1. Sissingh, G. J., "The effect of Induced Velocity Variation on Helicopter Rotor Damping in Pitch or Roll", Aeronautical Research Council (Great Britain), A.R.C. Technical Report C.P. No. 101 (14,757), 1952.
2. Ormiston, R. A. and Peters, D. A., "Hingeless Helicopter Rotor Response with Non-Uniform Inflow and Elastic Blade Bending", *Journal of Aircraft*, Vol. 9, No. 10, O. 1972, pp. 730-736.
3. Peters, D. A., "Hingeless Rotor Response with Unsteady Flow", presented at the AHS/NASA—Ames Specialists Meeting on Rotorcraft Dynamics, NASA SP—362, February 1974.
4. Pitt, D. M., *Rotor Dynamic Inflow Derivatives and Time Constant from Various Inflow Models*, Doctor of Science Thesis, Washington University, December 1980.
5. Pitt, D. M. and Peters, D. A., "Theoretical Prediction of Dynamic Inflow Derivative", Vertica, Vol. 5, No. 1, March 1981, pp 21 – 34.
6. Pitt, D. M. and Peters, D. A., "Rotor Dynamic Inflow Derivatives and Time Constants from Various Inflow Models", 9th European Rotorcraft Forum, Stresa, Italy, September 13 – 15, 1983.
7. Peters, D. A. and He, C-J, "A Finite-State Induced-Flow Model for Rotors in Hover and Froward Flight", proceedings of the 43rd Annual National Forum of the American Helicopter Society, St. Louis, MO, May 1987.
8. Nelson, Adria M., *A State-Space, Two-Dimensional Potential Flow Wake Model from a Galerkin Approach*, Master of Science Thesis, Washington University, May 2001.
9. Morillo, J. A., *A Fully Three-Dimensional Unsteady Rotor Inflow Model from a Galerkin Approach*, Doctor of Science Thesis, Washington University, December 2001.
10. He, C-J, *Development and Application of a Generalized Dynamic Wake Theory for Lifting Rotors*, Doctor of Philosophy Thesis, Georgia Institute of Technology, July 1989.
11. Gautschi, W., "Computational Aspects of Three-Term Recurrence Relations", *SIAM Review*, Vol. 9, 1967, pp 24 – 82.
12. Gradshteyn, I. S. and Ryzhik, I. M., *Table of Integrals, Series, and Products*, Academic Press, New York, 1980.
13. Abramowitz, M. and Stegun, I. A., *Handbook of Mathematical Functions*, Dover Publications, New York, 1970.

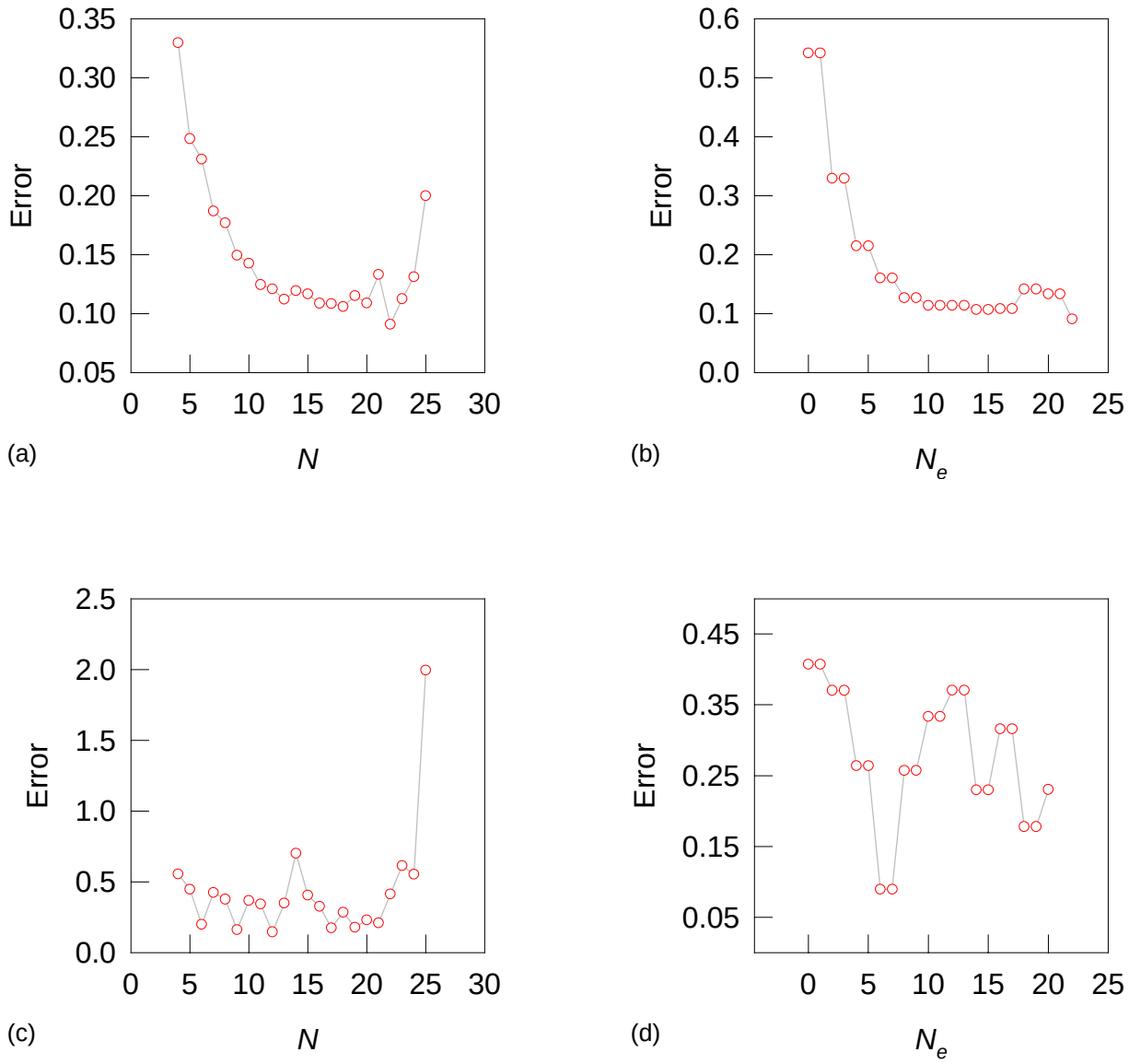


**Figure 2.** **On-disc error analysis comparing results from state-space model and convolution integral. Pressure distribution $P = -\Phi_0^0$ with $\omega = 0$ ((a) and (b)) and $\omega = \infty$ ((c) and (d)). The state-space model in (a) and (c) uses various but equal numbers of even and odd terms ($N$) in the zeroth harmonic; In (b) it has 22 odd terms and various number of even terms ($N_e$) in the zeroth harmonic; In (d) it has 20 odd terms and various number of even terms ($N_e$) in the zeroth harmonic. Responses are evaluated with $z = 0^-$ (on the actuator plane), $\chi = 0$ (axial inflow), $\bar{\psi} = 0^\circ, 180^\circ$ (along fore-and-aft axis).**

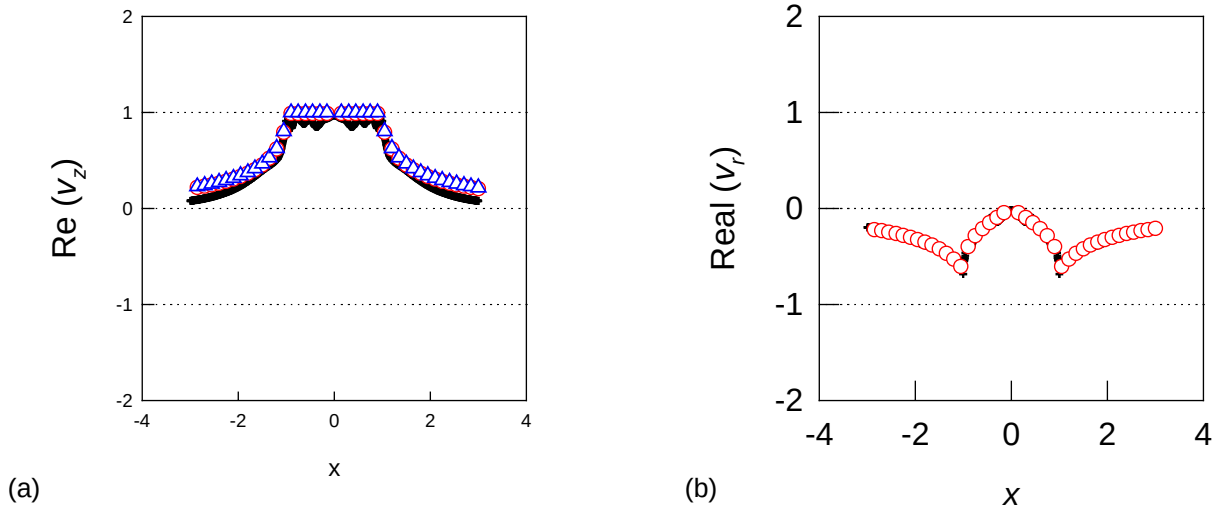


**Figure 3.** **Frequency response of pressure distribution $P=-\Phi_0^0$ with $\omega=0$. All other components of induced velocities are zeroes. Both number of odd and even terms included in state-space model are 11. Highest power of radial polynomials is 22. Responses are evaluated with $z=0^-$ (on the actuator plane), $\chi=0$ (axial inflow), $\bar{\psi}=0^\circ,180^\circ$ (along fore-and-aft axis). Red circles present values of convolution integral results at locations; blue triangles present results of closed-form solution; and black dots present results obtained by Galerkin approach.**

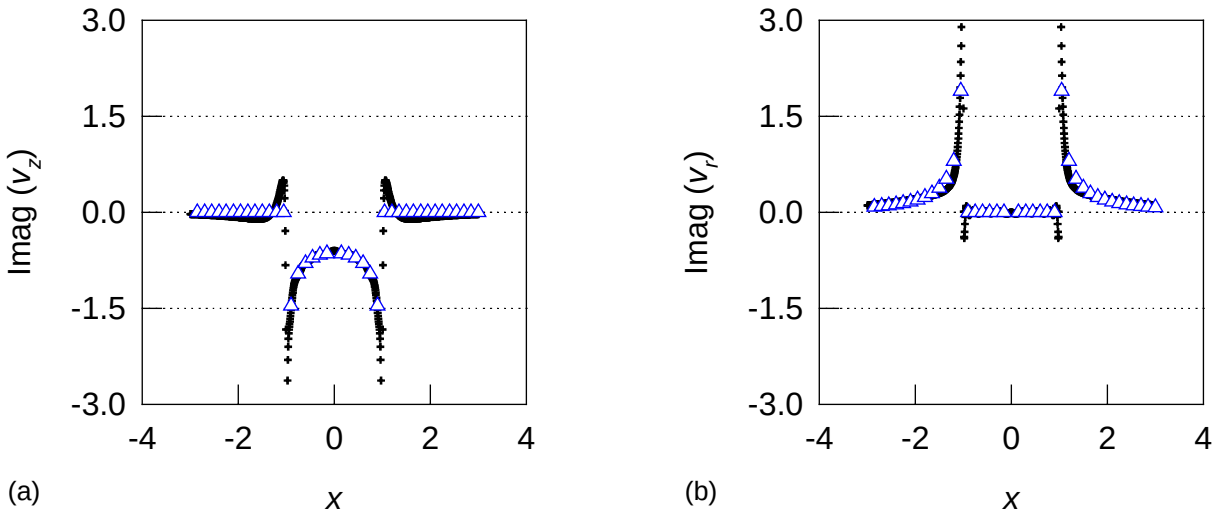


**Figure 4.** **Frequency responses of pressure distribution $P=-\Phi_0^0$ with $\omega=\infty$. All other components of induced velocities are zeroes. Number of odd terms included in the state-space model is 10; Number of even terms is 3. Highest power of radial polynomials is 20. Responses are evaluated with $z=0^-$ (on the actuator plane), $\chi=0$ (axial inflow), $\bar{\psi}=0^\circ,180^\circ$ (along fore-and-aft axis). Blue triangles present results of closed-form solution; and black dots present results obtained by Galerkin approach.**

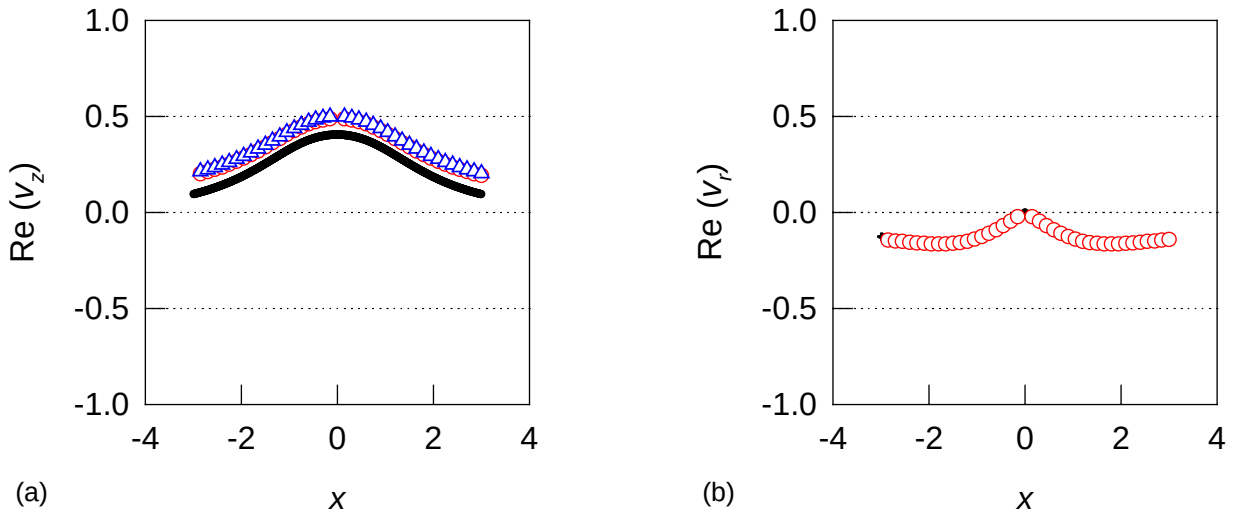


**Figure 5.** **Frequency response of pressure distribution $P=-\Phi_0^0$ with $\omega=0$. All other components of induced velocities are zeroes. Both number of odd and even terms included in state-space model are 11. Responses are evaluated with $z=-1$ (one radius above the actuator plane), $\chi=0$ (axial inflow), $\bar{\psi}=0^\circ,180^\circ$ (along fore-and-aft axis). Red circles present values of convolution integral results at locations; blue triangles present results of closed-form solution; and black dots present results obtained by Galerkin approach.**

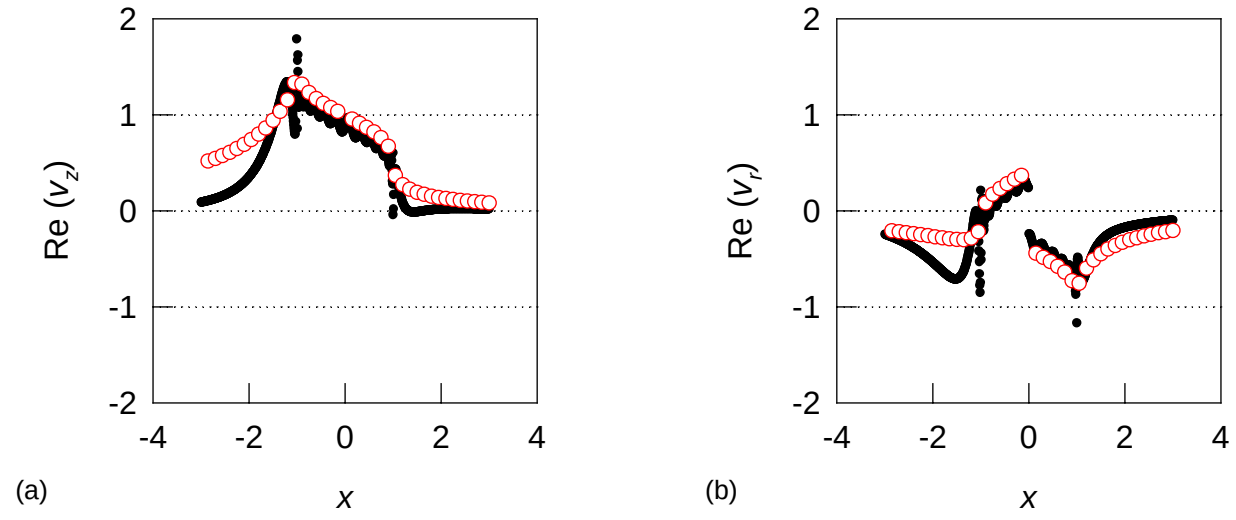


**Figure 6.** **Frequency responses of pressure distribution $P=-\Phi_0^0$ with $\omega=4.0$. All other components of induced velocities are zeroes. Number of odd terms included in the state-space model is 12; Number of even terms is 5. Highest power of radial polynomials is 24. Responses are evaluated with $z=0^-$ (on the actuator plane), $\chi=45^\circ$, $\bar{\psi}=0^\circ,180^\circ$ (along fore-and-aft axis). Red circles present results of convolution integral; and black dots present results obtained by Galerkin approach.**

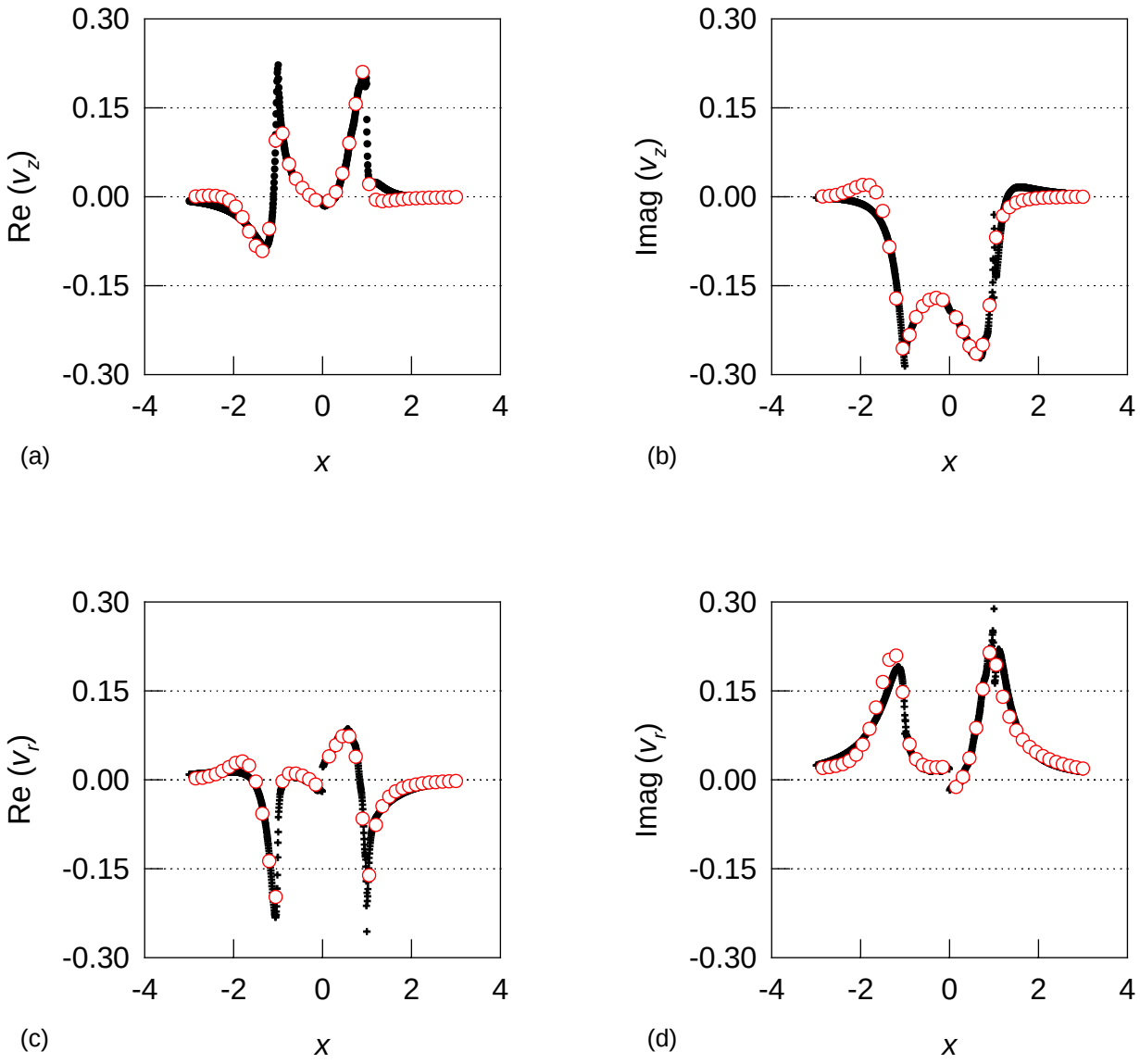


**Figure 7.** **Frequency responses of pressure distribution $P = -\Phi_0^0$ with skew angle $\chi = 45^\circ$, frequency $\omega = 4$. Number of odd terms is 12; number of even terms is 4. Highest power of radial polynomials is $N_r = 24$. Evaluation is performed on the actuator plane, $z = 0^-$. Plots (a) and (b) are real and imaginary parts, respectively, of vertical component of induced velocity. Plots (c) and (d) are those of radial component of induced velocity. Red circles present values of convolution integral results at locations; and black dots present results obtained by Galerkin approach.**

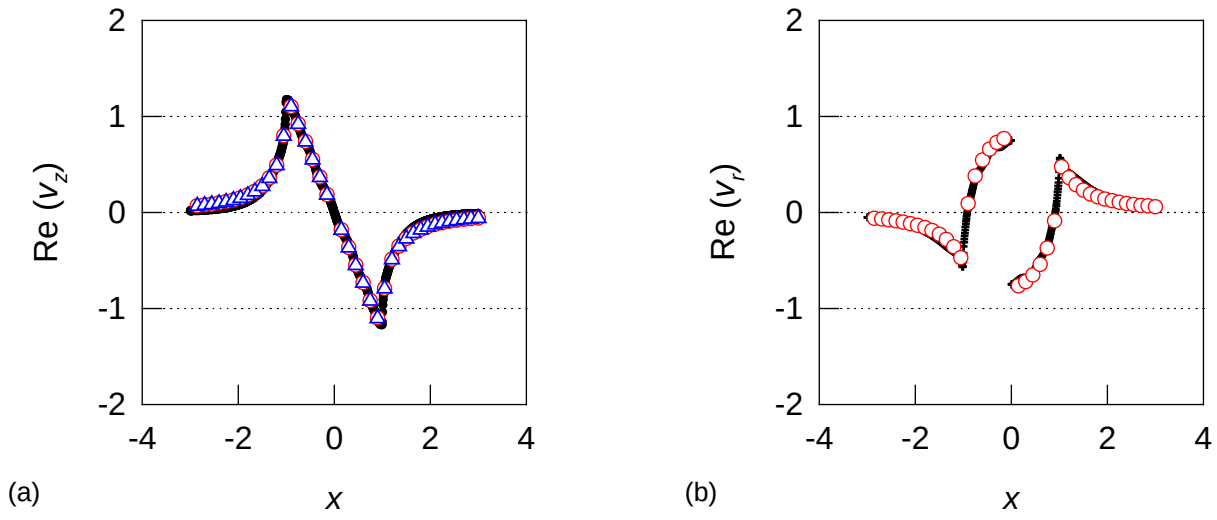


**Figure 8.** **Frequency response of pressure distribution $P=-\Phi_1^1$ with $\omega=0$. All other components of induced velocities are zeroes. Numbers of odd and even terms included in state-space model are 11 and 10, respectively. Highest power of radial polynomial is 21. Responses are evaluated with $z=0^-$ (on the actuator plane), $\chi=0$ (axial inflow), $\bar{\psi}=0^\circ,180^\circ$ (along fore-and-aft axis). Red circles present values of convolution integral results at locations; blue triangles present results of closed-form solution; and black dots present results obtained by Galerkin approach.**

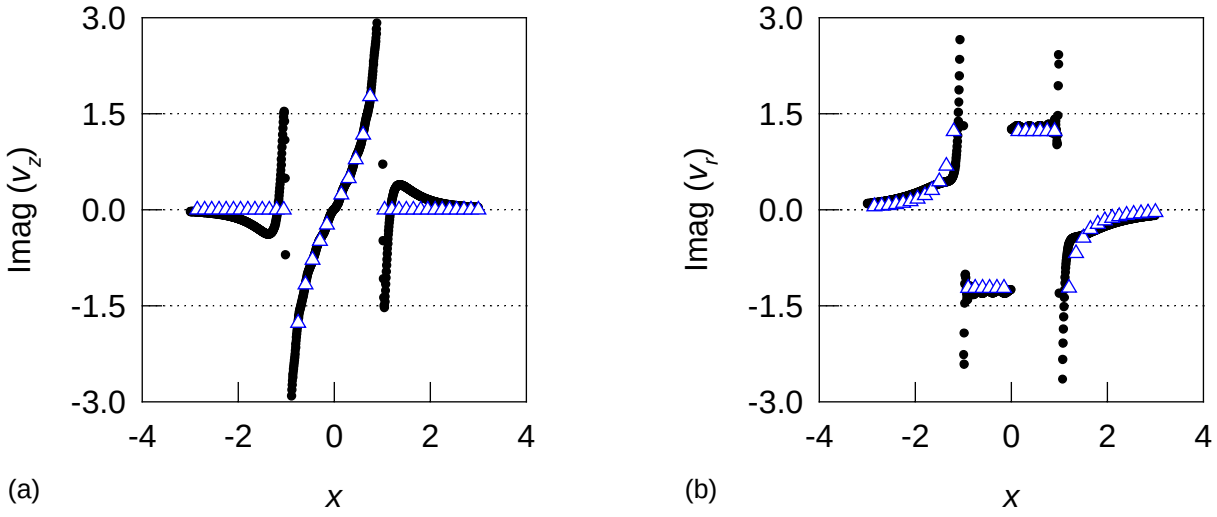


**Figure 9.** **Frequency response of pressure distribution $P=-\Phi_1^1$ with $\omega=\infty$. All other components of induced velocities are zeroes. Numbers of odd and even terms included in state-space model are 12 and 4, respectively. Highest power of radial polynomial is 23. Responses are evaluated with $z=0^-$ (on the actuator plane), $\chi=0$ (axial inflow), $\bar{\psi}=0^\circ,180^\circ$ (along fore-and-aft axis). Red circles present values of convolution integral results at locations; blue triangles present results of closed-form solution; and black dots present results obtained by Galerkin approach.**